Revista Mexicana de Ingeniería Química
ISSN: 1665-2738
amidiq@xanum.uam.mx
Universidad Autónoma Metropolitana
Unidad Iztapalapa
México

Yocupicio, R.I.; Díaz de León, J. N.; Zepeda, T.A.; Fuentes, S.
STUDY OF CoMo CATALYSTS SUPPORTED ON HIERARCHICAL MESOPOROUS ZEOLITES FOR HYDRODESULFURIZATION OF DIBENZOTHIOPHENE
Revista Mexicana de Ingeniería Química, vol. 16, núm. 2, 2017, pp. 503-520
Universidad Autónoma Metropolitana Unidad Iztapalapa
Distrito Federal, México

Vol. 16, No. 2 (2017) 503-520

Catálisis, cinética y reactores

Revista Mexicana de Ingeniería Química

STUDY OF CoMo CATALYSTS SUPPORTED ON HIERARCHICAL MESOPOROUS ZEOLITES FOR HYDRODESULFURIZATION OF DIBENZOTHIOPHENE

ESTUDIO DE CATALIZADORES CoMo SOPORTADOS SOBRE ZEOLITAS MESOPOROSAS JERÁRQUICAS PARA HIDRODESULFURACIÓN DE DIBENZOTIOFENO

R.I. Yocupicio*, J. N. Díaz de León, T.A. Zepeda, S. Fuentes

Centro de Nanociencias y Nanotecnología, Universidad Nacional Autónoma de México, Ensenada, Baja California, C.P. 22860, México.

Received November 15, 2016; Accepted January 26, 2017

Abstract

Three zeolites systems (ZSM-5, Faujasite Y, Mordenite) were prepared by using a supramolecular surfactant assembly method. Samples were labeled depending on the obtained phase, F (faujasite) and M (ZSM-5), 1 for (Dimethyloctadecyl[3-(trimethoxysilyl)propyl] ammonium chloride (DMOTPAC) and 2 by using cetyltrimethylammonium bromide-polyethylene glycol (CTAB-PEG). The textural properties for supports exhibited a unimodal pore size distribution around 3.9 nm. The TEM images showed the formation of different structures and morphologies, depending on the type of sample. The TPD of NH_3 results indicated a clear variation in the quantities of acid sites following the trend F2>F1>M2>M1. These materials were used to support Co-Mo sulfides and they were tested in the hydrodesulfurization (HDS) of dibenzothiophene (DBT). The CoMo catalysts showed the activities trend: CoMo/M1>CoMo/M2>CoMo/F1> CoMo/F2. This behavior resulted in agreement with length and stacking of MoS_2 slabs as well as with the NO adsorption amount. The tendency displayed by the surface acidity resulted inverse to the HDS activity and also was inversely proportional to the length and stacking of MoS_2 slabs. Thus, the highest the acid sites amount the lowest the slab length and stacking.

Keywords: synthesis, hierarchical, zeolite, mesoporosity, acidity.

Resumen

Tres sistemas zeolíticos (ZSM-5, Faujasita-Y, Mordenita) se prepararon por el método de ensamblaje supramolecular con surfactantes. Las muestras se etiquetaron de acuerdo con la fase obtenida, F (Faujasita) y M (ZSM-5), 1 para Cloruro de dimetiloctadecil[3-(trimetoxisilil)propil]amonio (DMOTPAC) y 2 para bromuro de hexadeciltrimetilamonio-Polietilenglicol (CTAB-PEG). Las propiedades texturales de los soportes mostraron una distribución de poros unimodal alrededor de 3.9 nm. Las imágenes de TEM mostraron la formación de diferentes estructuras y morfologías dependiendo del tipo de muestra. El análisis por TPD de NH_3 indicó una variación en la cantidad de sitios ácidos siguiendo la siguiente secuencia: F2>F1>M2>M1. Estos materiales se usaron como soportes de sulfuros de Co-Mo y se evaluaron en hidrodesulfuración (HDS) de dibenzotiofeno (DBT). Los catalizadores mostraron la siguiente tendencia en actividad catalítica: CoMo/M1>CoMo/M2>CoMo/F1>CoMo/F2. Esta tendencia resultó de acuerdo con la longitud y el apilamiento de las laminillas de MoS_2 así como con las pruebas de adsorción de NO. La tendencia mostrada por la acidez superficial resultó inversa a la actividad en HDS (M1>M2>F2>F1) la longitud y el apilamiento de las laminillas de MoS_2. En este sentido, a mayor cantidad de sitios ácidos, menor longitud y apilamiento de las laminillas.

Palabras clave: síntesis, jerárquica, zeolita, mesporosidad, acidez.

1 Introduction

Requirements for higher quality of fuels and strict environmental legislation on harmful emissions have motivated that more basic and applied research is being conducted in the hydrotreating of petroleum fractions. The sulfur specification for ultra-low sulfur diesel (ULSD) fuel has been introduced in Mexico and

* *Corresponding author. E-mail*: ryocu@cnyn.unam.mx
Tel. +(52) 6461071431, Fax: + (52) 6461744603

ratified in 2016 (D.O.F. 2016) by mean of the official standard NOM-016-CRE-2016; this established a maximum of 15 ppm sulfur content in diesel fuel. The present strategy in the oil industry is to process heavier oil stocks while keeping quality and ultra-low sulfur content of fuels. So, there is a challenge for developing new catalysts or improving actual materials as well as for designing of more efficient processes. The most common combinations of active metals in hydrotreating catalysts are CoMo, NiMo and NiW families commonly supported on alumina (H. Topsøe *et al.*, 1996). Widespread use of alumina in hydrotreating is essentially due to optimal textural and mechanical properties obtained at low cost (Breysse *et al.*, 2003). New methods with the intent to obtain highly dispersed active phase have been proposed (Choi *et al.*, 2004; Scott *et al.*, 2015; Munguía-Guillén *et al.*, 2016). Even so, new materials have been researched as supports of hydrotreating catalysts which include carbon, titania, siliceous materials, zeolites, and clays (Alonso-Nunez *et al.*, 2012; Ramirez *et al.*, 1989; Dugulan *et al.*, 2013; Huirache-Acuna *et al.*, 2014; Pawelec *et al.*, 2008; Trejo *et al.*, 2014) and some mixed oxides like Titania-Alumina, γ-Al_2O_3-αGa_2O_3, MgO-TiO_2 and the AlTiMg oxide system (Tavizon-Pozos *et al.*, 2016; Díaz de León 2016; Cruz Pérez *et al.*, 2016; Cervantes-Gaxiola *et al.*, 2013). The use of new supports materials is mainly attributed to the necessity of finding more active catalysts with CoMoS phases in their structure. The CoMoS phase is a MoS_2-like structure with promoter atoms located at the edges planes of MoS_2 (H. Topsøe *et al.*, 1996) which is considered the active HDS phase.

Zeolites are one of the most used catalysts in many processes. Features like microporosity, medium and strong acidity and excellent textural properties as well as stability, make them good catalysts for several reactions. It has been reported the use of zeolites in reactions catalyzed by acid sites as hydration of cyclohexene, NO reduction, alkylation of benzene, aromatization, and so on (Ishida 1997; Iwamoto *et al.*, 1991; Feng & Keith Hall 1997; Corma *et al.*, 2000; Jentoft *et al.*, 1998). However, the intrinsic microporosity observed in this kind of materials has limited their use in hydrotreating reactions. Typical molecules as DBT has been reported to have molecular diameter near to 11.6 Å (Moosavi *et al.*, 2012), therefore they cannot diffuse through the structure of zeolitic materials (Perez-Ramirez *et al.*, 2008). In recent years, research has been focused on overcoming the limitations of micropores providing shorter diffusion paths (Tosheva & Valtchev 2005) through the synthesis of nanosized zeolites or generating mesopores. These methods include using hard templates (Egeblad *et al.*, 2008), organosilane surfactants or soft polymers (Serrano *et al.*, 2006; Srivastava *et al.*, 2006), post-synthesis zeolites desilication and desalumination (Groen *et al.*, 2007) or pseudomorphic transformation of silica gel (Choi *et al.*, 2009). The intensive research provided by potential application of that materials brought a new definition of mesostructured zeolites; that is "hierarchical zeolites". This kind of material has attracted huge interest since the beginning of 21st century, emphasizing that the only one necessary feature to be included in this category is that they contain additional porosity (meso or macro) to microporosity of the zeolite structure (Egeblad *et al.*, 2008; Perez-Ramirez *et al.*, 2008). Several reactions with molecules were tested with the intention to prove the impact of additional zeolite porosity in the transport of larger molecules; in this way benzene alkylation, methanol to propylene conversion, n-hexadecane aromatization, triisopropyl benzene cracking, among others, were proved (Chica *et al.*, 2009; Christensen *et al.*, 2003; Lei *et al.*, 2006; Mei *et al.*, 2008).

The use of zeolites in industrial HDS catalysts has been reported and it has been suggested that zeolites help to improve the catalytic activity and stability of catalysts (Yoshinari *et al.*, 1996; Fujikawa *et al.*, 1998). In the same way, it is well-known that hydrotreatment catalysts possess acid features (Gates *et al.*, 1979). On the other hand, it has been reported that hydrogen spillover can enhance the hydrogenating capacity (H. Topsøe *et al.*, 1996) and the design of new mesoporous zeolites can facilitate the design of catalysts with catalytic active sites in micropores and mesopores that take advantage of hydrogen spillover (Tang *et al.*, 2013).

The use of zeolites in industrial HDS catalysts has been reported and it has been suggested that zeolites help to improve the catalytic activity and stability of catalysts (Yoshinari *et al.*, 1996; Fujikawa *et al.*, 1998). In the same way, it is well-known that hydrotreatment catalysts possess acid features (Gates *et al.*, 1979). On the other hand, it has been reported that hydrogen spillover can enhance the hydrogenating capacity (H. Topsøe *et al.*, 1996) and the design of new mesoporous zeolites can facilitate the design of catalysts with catalytic active sites in micropores and mesopores that take advantage of hydrogen spillover (Tang *et al.*, 2013).

2 Experimental

2.1 Preparation of supports

The MFI zeolite (labeled M1) was hydrothermally synthesized with (Dimethyloctadecyl[3-(trimethoxysilyl)propyl] ammonium chloride as a mesopore-directing agent like those proposed by Choi *et al.*, (2006) and Shetti *et al.*, (2008). In this synthesis procedure for M1 we used 3.7 g of mesoporogen (Dimethyloctadecyl[3-(trimethoxysilyl)propyl] ammonium chloride (72% in methanol Sigma-Aldrich)) (DMOTPAC), 2.66 g of structure director agent (SDA) tetra propylammonium bromide (TPABr 98% Sigma-Aldrich), 0.77 g of NaOH (98% Sigma-Aldrich). The reactants have been fully dissolved in 36.3 g of H_2O and mixed with 21.4 g of sodium silicate solution (25% Wt. of SiO_2, 10.6% wt. Na_2O, Sigma-Aldrich) for 20 minutes with vigorous stirring. Then a solution containing 0.48 g of sodium aluminate (98% Sigma-Aldrich) in 26.6 g of H_2O was added dropwise, finally 26 g of a solution 10% wt. H_2SO_4 were added under vigorous stirring. The mixture was heated at 150 °C for 4 days in a Teflon-coated stainless steel autoclave.

The mixed phases of MFI and mordenite (labelled M2) was synthesized by the same procedure than the M1 sample with the difference that the mesoporogen were changed to 3.1 g of Cetyltrimethylammonium bromide (CTABr 98%, Sigma-Aldrich) and 0.5 g of polyethylene glycol 20000 (PEG 2000, Sigma-Aldrich), while the SDA was increased to 3.2 g.

The faujasite "Y" zeolite (labeled F1) was synthesized as Ginter *et al.*, (1992) proposed; this method is divided into two steps:

1. Seed Gel: 19.95 g of H_2O, 4.07 g of NaOH (98%, Sigma-Aldrich) and 2.09 g of sodium aluminate (98%, Sigma-Aldrich)] were mixed and stirred in a 50 mL plastic bottle until dissolved. Then 22.72 g of sodium silicate (a solution of 25% wt. SiO_2, 10.6% wt. Na_2O, Sigma-Aldrich) were added stirring moderately for at least 10 minutes; after mixing, the bottle was covered and the solution aged at room temperature for 1 day.

2. In a plastic bottle, the second solution with 32.7 g of H_2O, 0.035 g de NaOH, 3.27 g of sodium aluminate, 3 g of DMOTPAC (72% in ethanol, Sigma-Aldrich) was prepared and stirred until dissolution. Then 35.6 g of sodium aluminate were added stirring vigorously until the gel appeared somewhat smooth and then slowly 4.1 g of seed gel was added under vigorous stirring.

A second faujasite Y zeolite (labeled F2) was synthesized by the same method like F1, but the mesoporogen was changed to 2.2 g of CTABr (98% Sigma-Aldrich) with 0.36 g of PEG 20000 (Sigma-Aldrich). The two samples were incubated for a one day in a 300 mL polypropylene bottle (sealed) at room temperature and then were crystallized at 100 °C for 6 h.

A second faujasite Y zeolite (labeled F2) was synthesized by the same method like F1, but the mesoporogen was changed to 2.2 g of CTABr (98% Sigma-Aldrich) with 0.36 g of PEG 20000 (Sigma-Aldrich). The two samples were incubated for a one day in a 300 mL polypropylene bottle (sealed) at room temperature and then were crystallized at 100 °C for 6 h.

2.2 Preparation of the catalysts

The catalysts were prepared by simultaneous impregnation using the pore filling method. All catalysts were developed with the nominal metallic composition of 4.0 and 13 wt. % of Co and Mo respectively. The precursors for impregnation were ammonium molybdate tetrahydrate $(NH_4)_6Mo_7O_{24}\cdot 4H_2O$ (81-83% Sigma-Aldrich) and cobalt nitrate hexahydrate $Co(NO_3)_2\cdot 6H_2O$ (98% Sigma-Aldrich). The Co and Mo solutions were stabilized in aqueous solution by use of citric acid (99% Sigma-Aldrich) in a 1:1 molar ratio with Co. All samples was dried for 12 hours at room temperature and then at 60 °C for 12 hours, followed by calcination at 450 °C for 4 hours.

2.3 Characterization methods

2.3.1 X-Ray diffraction

The X-ray diffraction (XRD) patterns of the oxide catalysts were recorded on a Philips X-Pert MPD diffractometer, using monochromatic Cu Kα radiation (λ= 0.154056 nm). The diffractograms were recorded in the 2θ range of 5-40°.

2.3.2 Nitrogen adsorption-desorption

The textural properties of the supports and oxide catalysts were determined by the nitrogen adsorption-desorption measurements. These measurements were carried out at -196 °C with equipment ASAP 2000 from Micromeritics. Samples were degassed under

argon flow at 300 °C for 4 h before nitrogen adsorption. The surface area measurements were performed according to the Brunauer-Emmett-Teller (BET) method on the relative pressures $0.05 < P/P_0 < 0.30$. The average pore diameter was calculated following the Barret-Joyner-Halenda method (BJH) using the desorption branch of the N_2 isotherm. The cumulative pore volume was obtained from the isotherms at $P/P_0 = 0.99$.

2.3.3 Transmission electron microscopy

TEM micrographs have been achieved in a JEOL JEM-2010 instrument. The sulfide catalysts and oxide supports were suspended in isopropyl alcohol as a solvent to be deposited on lacey carbon (440 mesh) Cu grid holders. The average stack length ($\overline{L}$) and the stacking degree ($\overline{N}$) were calculated for examination of more than 800 particles. The statistical results were obtained according to Eqs. (1) and (2) (Knudsen *et al.*, 1999; Díaz de León *et al.*, 2010).

$$\overline{L} = \frac{\sum_{i=1}^{n} nili}{\sum_{i=1}^{n} ni} \quad (1)$$

$$\overline{N} = \frac{\sum_{i=1}^{n} niNi}{\sum_{i=1}^{n} ni} \quad (2)$$

Where *li* is the length of slab *i*, *ni* the number of particles with a *li* length or *Ni* layers, and *Ni* the number of layers in the particle *i*.

2.3.4 Temperature programmed desorption of NH_3 (TPD-NH_3)

The acid strength of the oxide catalysts was determined by TPD-NH_3 measurements using the Micromeritics TPD/TPR 2900 equipment. The sample (500 mg) was previously degassed in a He flow (Air Liquide, 99.996%) at 300 °C for 1 h and then it was ammonia-saturated by flowing 5% NH_3/He stream at 100 °C for 1 hour. After equilibration in Ar flow for 30 minutes at 100 °C, the catalyst was heated at a linear rate of 10 °C min^{-1} from 100 °C to 600 °C, and the detector signal of ammonia desorption was recorded.

2.3.5. DRIFTS spectra of adsorbed NO

The DRIFTS spectra of adsorbed NO were obtained with a Cary 600 Series FTIR spectrometer, using a Harrick HVCDRP cell that allows *in situ* treatments with different gasses at temperatures up to 500 °C. The interferograms were obtained after 100 scans using a KBr spectrum as background. About 30 mg of finely grounded powder was placed in a sample holder and degassed under Vacuum at 400 °C for 2 hours. Then the samples were cooled at room temperature, pressurized to 50 mbar of NO and stabilized for 20 minutes before to take the spectra.

2.3.6 Catalytic activity measurements

All catalysts were thoroughly grounded in a mortar and passed through the 80-125 sieves, before the catalytic runs. The oxide catalysts (ca. 0.235 g) were also activated by an ex-situ sulfidation treatment performed in a U-shape glass flow reactor. The samples were flushed in a mixture (H_2/H_2S 15 vol. % H_2S,) at a flow of 40 mL min^{-1} and the temperature was increased to 400 °C (reaching this temperature in 37 minutes) and maintained for 1 h, The sample was then cooled down to room temperature and transferred to the reactor under Ar atmosphere to avoid contact with air. Catalytic activity tests were measured in a batch Parr reactor charged with c.a. 0.227 g of DBT (500 ppm of S) dissolved in 100 mL of n-hexadecane. The reactor was additionally purged with nitrogen to eliminate oxygen traces. The reaction was carried out for 5 h at 320 °C under a hydrogen pressure of 5.5 MPa and stirred at 700 RPM. The reaction products were analyzed by GC on a Perkin-Elmer XL device using a 30 m long Agilent J&W HP-5 capillary column. The reaction products detected by GC were: biphenyl (BP), cyclohexylbenzene (CHB), dicyclohexyl (DCH) and traces of tetrahydrodibenzothiophene (THDBT). The mass balance in all experiments was within the 99.0-99.98% range. The catalytic activity was expressed by the initial reaction rate which was determined from the DBT conversion (X_{DBT}) as a function of the time and catalysts quantity (mol DBT transformed per second and per gram of catalyst) according to Eq. (3). The DDS and HYD selectivity were calculated according to Eqs. (4) and (5), respectively.

$$XDBT = \frac{(CHB + BP + DCH + THDBT) \times 100\%}{(DBT + CHB + BP + DCH + THDBT)} \quad (3)$$

$$DDS = \frac{(BP) \times 100\%}{(CHB + BP + DCH + THDBT)} \quad (4)$$

$$HYD = \frac{(CHB + DCH + THDBT) \times 100\%}{(CHB + BP + DCH + THDBT)} \quad (5)$$

Table 1. Reaction rates and selectivity for all catalysts tested. Selectivity results obtained at 30% of conversion.

Catalyst	Initial reaction rate $\times 10^{-8}$ molDBT(gCAT·s)$^{-1}$	Selectivity (%) DDS	HYD	HYD/DDS
CoMo/M1	18.1±0.58	88	12	0.14
CoMo/M2	16.4±0.49	89	11	0.12
CoMo/F1	14.3±0.44	92	8	0.09
CoMo/F2	12.1±0.40	90	10	0.11

3 Results

3.1 Catalytic activity evaluation

The specific reaction rates (rDDS and rHYD) and selectivities obtained for the sulfide catalysts are presented in Table 1. It is well known that HDS of DBT can proceed by two parallel pathways. The direct desulfurization (DDS), leading to biphenyl and the two steps hydrogenation of the aromatic rings (HYD) producing some intermediates like tetra or hexa hydro dibenzothiophene followed by the S-C bond break and hydrogenation to obtain subsequently cyclohexylbenzene (CHB) and bicyclohexyl (BCH). We observed that the DDS pathway resulted in the predominant reaction route in all catalysts; this is intrinsic of the active phase and the DBT model molecule since it is well-known that the promotion of the MoS_2 phase by cobalt increase the DDS properties and DBT normally reacts throughout this pathway in catalysts with low hydrogenation properties (H. Topsøe *et al.*, 1996; Oballa 1994). Therefore, selectivity throughout this pathway resulted above 90% while HYD reached only 8 to 12% at 30% conversion. It was considered that this secondary reaction has not a direct influence on the HDS activity. Further studies about hydrotreating and hydrocracking reactions working together will be reported later.

The specific reaction rates (rDDS and rHYD) and selectivities obtained for the sulfide catalysts are presented in Table 1. It is well known that HDS of DBT can proceed by two parallel pathways. The direct desulfurization (DDS), leading to biphenyl and the two steps hydrogenation of the aromatic rings (HYD) producing some intermediates like tetra or hexa hydro dibenzothiophene followed by the S-C bond break and hydrogenation to obtain subsequently cyclohexylbenzene (CHB) and bicyclohexyl (BCH). We observed that the DDS pathway resulted in the predominant reaction route in all catalysts; this is intrinsic of the active phase and the DBT model molecule since it is well-known that the promotion of the MoS_2 phase by cobalt increase the DDS properties and DBT normally reacts throughout this pathway in catalysts with low hydrogenation properties (H. Topsøe *et al.*, 1996; Oballa 1994). Therefore, selectivity throughout this pathway resulted above 90% while HYD reached only 8 to 12% at 30% conversion. It was considered that this secondary reaction has not a direct influence on the HDS activity. Further studies about hydrotreating and hydrocracking reactions working together will be reported later.

3.2 XRD analysis

The XRD patterns for supports are shown in Fig. 1 A). It was observed several diffraction peaks in the analyzed range (5-40 2θ degrees) which indicate highly crystalline zeolites. The pattern obtained for M1 sample shows typical MFI signals at 7.9, 8.8 and 23.1 2θ degrees corresponding to (101), (020) and (051) planes respectively (ICDD No. 44-0003). These planes normally produce high-intensity reflections as it was observed in our sample.

The diffraction pattern for M2 sample showed mixed phases of mordenite and MFI structure, probably induced by the change in the synthesis procedure (2.1 section). The signals for M2 sample appeared around 9.6, 19.7, 22.4 and 25.8 2θ degrees. These peaks correspond to (200), (400), (150) and (202) planes of mordenite structure according to the ICDD No. 49-0924 phase. Also, it was possible to observe the signals c.a. 7.9, 8.8 and 23.1 2θ degrees assigned to (101), (020) and (051) reflections from the MFI structure as in the case of the M1 sample. The F1 and F2 samples showed characteristic faujasite Y diffractions. The signals for F1 and F2 sample appear around 6.1, 15.6 and 23.5 2θ degrees. These peaks correspond to (111), (331) and (533) planes of Faujasite Y structures according to ICDD No. 38-0238.

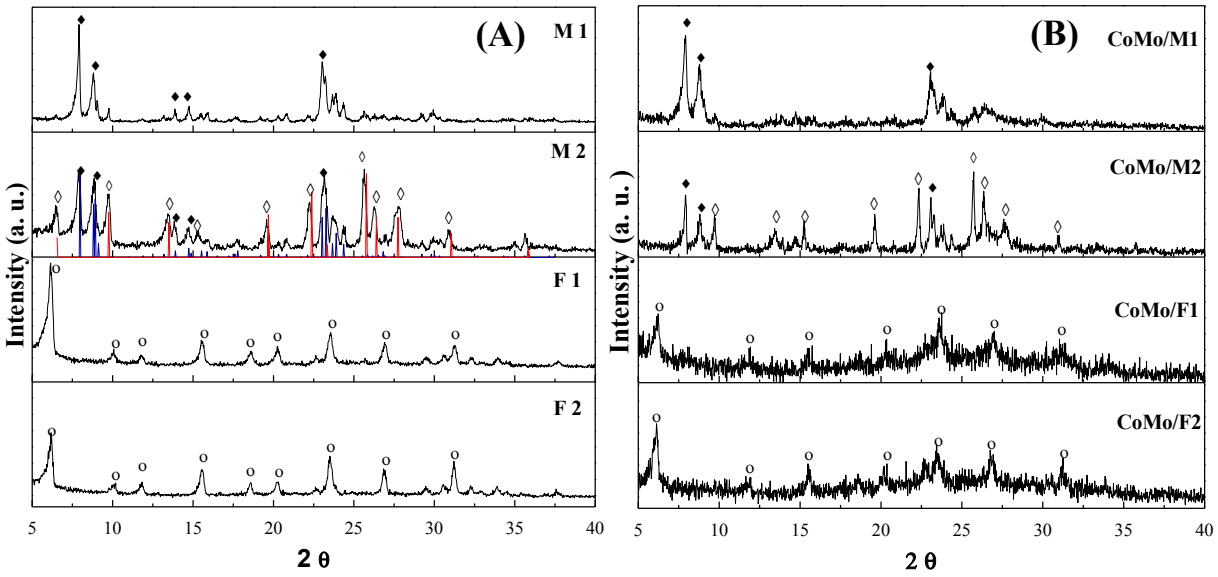

Fig. 1. (A) X-ray diffraction patterns of supports. (B) X-ray diffraction patterns of catalysts. ZSM-5 reflections are ♦, Mordenite reflections are ◊ and Faujasite Y reflections are o.

Table 2. Textural properties of supports and oxide catalysts

Sample	S_{BET} (m^2g^{-1})	V_p (cm^3g^{-1})	V_{mp} (cm^3g^{-1})	PD (nm)
M1	392	0.35	0.09	4
M2	389	0.29	0.16	4
F1	534	0.36	0.22	3.8
F2	380	0.3	0.22	3.8
CoMo/M1	214	0.18	0.06	3.8
CoMo/M2	151	0.12	0.06	4
CoMo/F1	199	0.16	0.06	3.8
CoMo/F2	150	0.1	0.05	3.8

The XRD patterns for the catalysts are shown in Figure 1.B. They resemble very similar to those obtained for the corresponding support. Although at simple view these patterns look as less crystalline materials. It was possible to identify the common signals MFI structure in CoMo/M1 sample. The diffraction pattern of CoMo/M2 sample showed signals of mordenite and MFI structures. Meanwhile, the CoMo/F1 and CoMo/F2 showed diffraction peaks at 6.1, 15.6 and 23.5 2θ degrees corresponding to (111), (331) and (533) planes of Faujasite Y structure. The lower intensity of catalysts than those of supports suggest that metals are dispersed on the zeolite. It has been reported that loading active phases decrease the support crystallinity (A. J. Duan *et al.*, 2010). There was not clear evidence of phases corresponding with molybdenum oxide or cobalt oxide that should appear at 2θ = 23.3º and 27.3º. Only a broad shoulder was observed in samples F1 and F2 in the 2θ = 20-30º region. Therefore, it was not possible to elucidate some particular signal for these Co or Mo oxides suggesting that they are well dispersed.

3.3 Textural properties

The BET surface area (S_{BET}), average pore diameter (P_D), total pore volume (V_p) and micropore volume (V_{mp}) are listed in Table 2 for supports and oxide catalysts. The surface areas of M1 and M2 samples were around 390 m^2g^{-1}. Meanwhile, the F1 showed surface areas around 500 m^2g^{-1}. These values are higher than those reported for ZSM-5 and faujasite Y by Ismagilov (Ismagilov *et al.*, 2009), and it is attributed to the presence of mesoporosity.

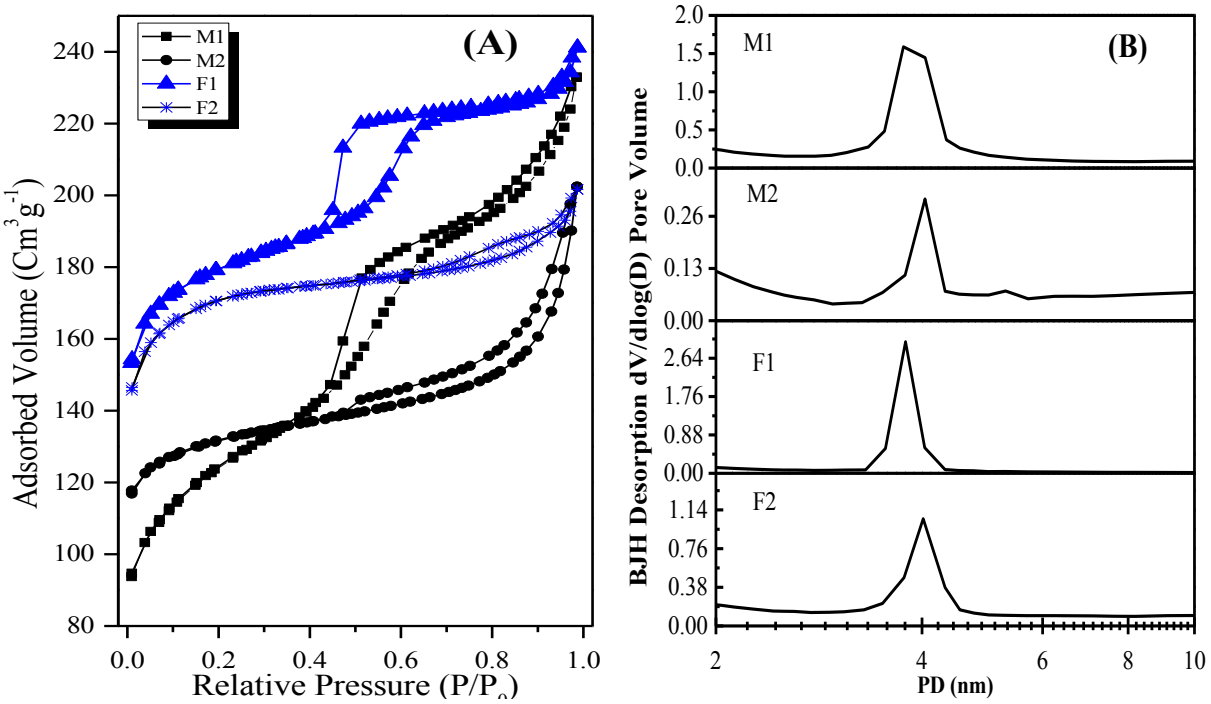

Fig. 2. A). N_2 adsorption-desorption isotherms for supports materials. B). Pore diameter distribution of bare supports.

On the other hand, the F2 sample displayed lower surface area than the F1 showing its low mesoporosity.

Values of micropore volume are close to those reported before for these zeolitic structures, MFI≈0.09, Mordenite≈0.14 and Fau≈0.22 cm^3g^{-1} (Ismagilov *et al.*, 2009; Morsli *et al.*, 2007). Hence, the increase in surface area and pore volume for supports can be attributed to mesopore formation. The analysis of N_2 adsorption-desorption isotherms (Figure 2A) resulted in IV type isotherms characteristics of mesoporous materials for M1 and F1. These supports clearly showed mesoporosity which is evident for the isotherm widening on the middle of relative pressure specifically in the P/P_0 = 0.45-0.65 range due to capillary condensation inside of the open mesopores; these isotherms are characteristics for cylindrical mesopores. Supports have the same total pore volume but the different volume of micro and mesopores derived from various zeolite structures (MFI and FAU). The isotherm for M2 material resulted of type II, characteristic of stacked sheets or shape slit mesopores. Capillary condensation in M2 sample showed a wider distribution of mesopores in the P/P_0 = 0.45-0.95 range of relative pressure compared to M1 and F1 materials. All isotherms showed adsorption at a relatively low pressure which is characteristic of materials with microporosity. In the same line, the order of micropore volume was as follows: F1 = F2 > M2 > M1. The pore size distributions of supports (Figure 2B) showed a similar distribution of mesopore diameter in the 3.8-4.4 nm range for all samples. The difference between materials was the volume of absorption, being higher in F1 and M1. As it was expected, the CoMo catalysts exhibited a clear reduction in the textural properties. The CoMo/M1 resulted with the higher S_{BET} (214 m^2g^{-1}) among series. The pore volume of samples was reduced in some cases more than 50%. Nevertheless, the intended use of this materials is for hydrodesulfurization reaction of DBT model molecule which can easily go inside these pore sizes taking into account the DBT molecule size of 11.6 Å, 7.4 Å and 3.6 Å (Moosavi *et al.*, 2012).

3.4 Transmission electron microscopy

TEM micrographs of supports are shown in Fig. 3. In micrographs of samples M1 and F1, Fig. 3a and Fig. 3c, respectively, was evident the presence of a well-defined mesostructure. It was reported that the synthesis procedure follows a supramolecular assembly of DMOTPAC in micelles inducing the

formation of uniform hollows in the final material (Choi *et al.*, 2006; Shetti *et al.*, 2008). The mesopore diameter observed was in the 3.8-4.0 nm range, in agreement with N2 adsorption-desorption data shown in Table 2. For samples synthesized with CTAB and PEG 20000 results indicated that F2 sample did not show hollows in the micrographs as M1 and F1 ones. On the other hand, M2 sample presented a bunch of nanorods without noticeable mesoporosity. However, the N2 adsorption-desorption analysis revealed that this is a mesostructured material. In this case, mesoporosity could be a consequence of inter nanorod spaces (De Leon *et al.*, 2014). Such type of interparticle spaces is different to those mesopores in M1 and F1. The nanostructure of sample M2 can be seen in Figure 4 where two images with lattices planes are shown. The left side of figure 4 demonstrates the interface between two parallel nanorods of mordenite sharing planes with d=0.89 nm, similar to the interplanar distance of (200) planes of Mordenite Zeolite. d= 0.9 nm (ICDD 49-0924). The right side of Figure 4 shows a crystal of ZSM-5 in M2 sample with interplanar distances corresponding to (111) and (101) diffraction planes for the ZSM-5 structure in the orthorhombic system. These results confirm the XRD observations (Figure 1A) that showed the presence of both types of zeolites in sample M2.

Selected HRTEM micrographs of sulfided catalysts are shown in Figure 5. The lattice planes identified in the micrographs were assigned to the diffraction planes of zeolites and metal sulfides in the catalysts. The CoMo/M1 and CoMo/M2 catalysts showed the (101) and (200) planes characteristic of the ZSM-5 and mordenite zeolitic framework respectively.

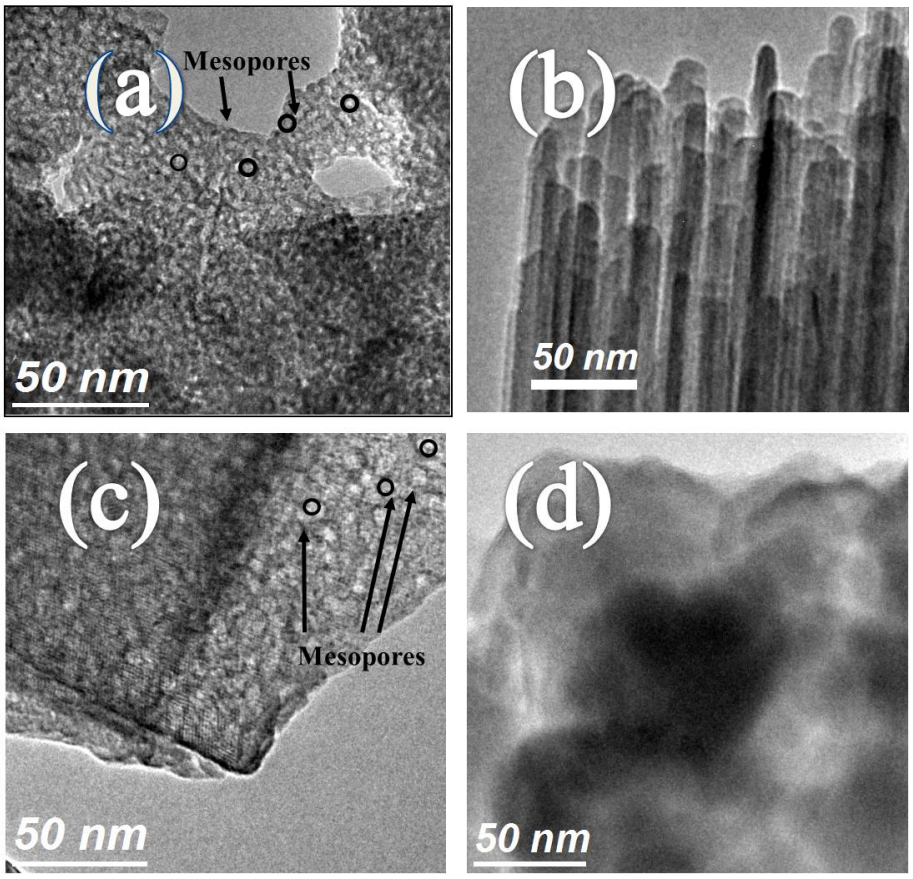

Fig. 3. TEM micrographs for the supports materials. (a) M1, (b) M2, (C) F1, (d) F2.

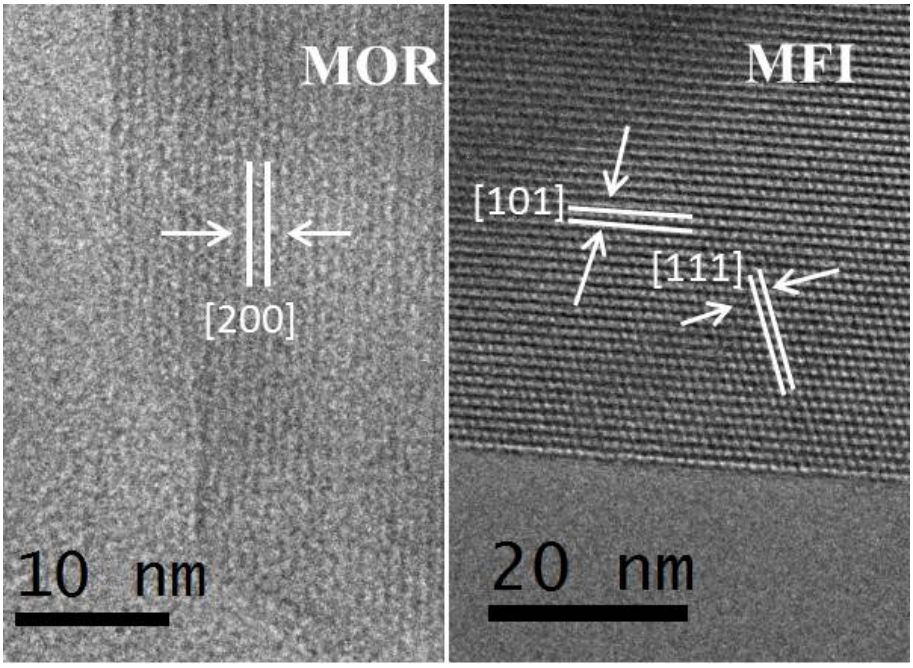

Fig. 4. Mordenite structure on left side and MFI structure on right side.

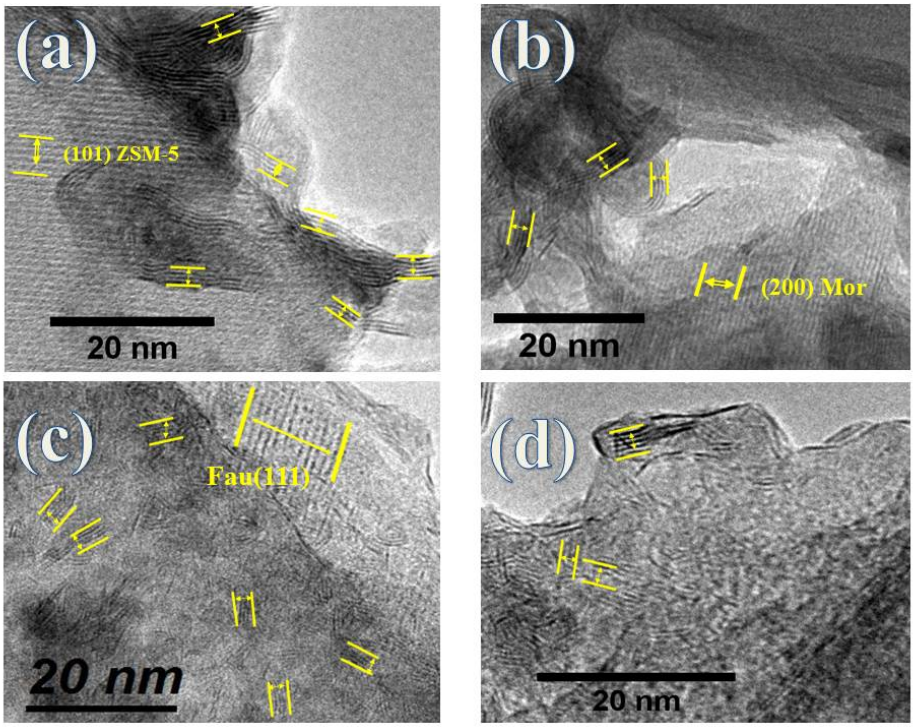

Fig. 5. TEM micrographs for sulfided catalysts. (a) CoMo/M1, (b) CoMo/M2, (c) CoMo/F1, (d) CoMo/F2.

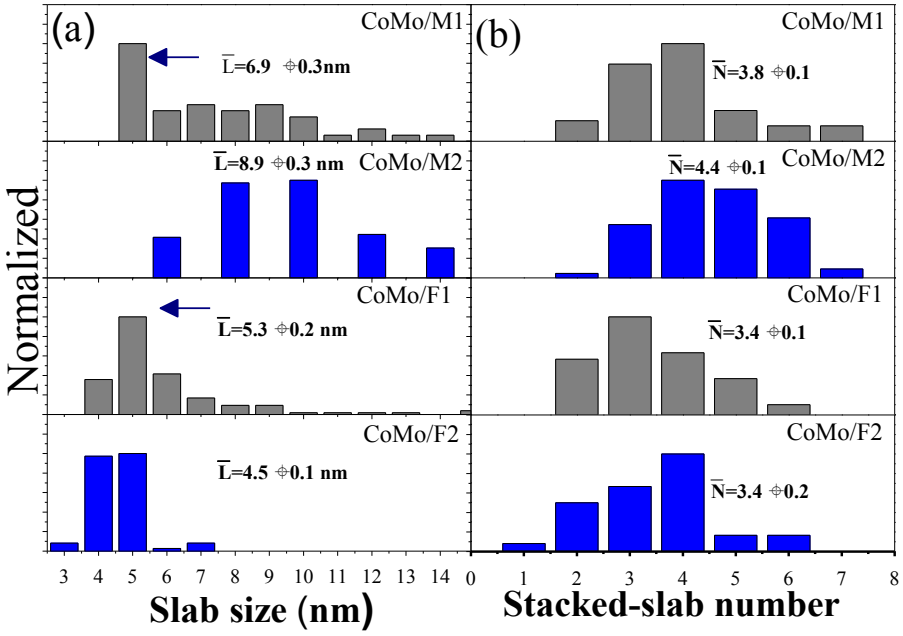

Fig. 6. Statistics of slab length (a) and stacked-slab number (b) of sulfided catalysts.

The morphological features of MoS_2 showed a different degree of stacked slabs of the active phase for all samples. The interplanar distances of that fringes were d=0.6±0.1 nm, corresponding to the most intense diffraction signal of (002) planes of MoS_2 phase (ICDD 01-070-9263). Micrographs showed multilayer stacks of sulfide phase which were distributed on the support surface, and they had slab length in the 4-8 nm range for catalysts supported on faujasite Y (CoMo/F1 and CoMo/F2) and in the 5-10 range for those supported on ZSM-5 and mordenite+ZSM-5 mixed phases supports.

The average slab length ($\overline{L}$) and stacked-slab number ($\overline{N}$) distributions were obtained by use the Eqs. (1) and (2) respectively and are presented in Figure 6. These distributions were extracted from statistical analysis of sulfided catalysts. The trend of $\overline{L}$ size and $\overline{N}$ resulted as follow: CoMo/M2 > CoMo/M1 > CoMo/F1 = CoMo/F2.

In the statistical analysis, the CoMo active phase in catalysts showed different distributions for the $\overline{L}$ and for the MoS_2 $\overline{N}$ depending on the support. The $\overline{L}$ values distribution of CoMo phase on Y faujasite showed broader distributions than metals on M1 and M2 supports being the CoMo/F2 catalyst with the most restrained distribution. On the contrary, the CoMo/M2 showed the widest distribution and the largest $\overline{L}$ value.

The stacking number distribution results revealed that catalysts CoMo/F1 and CoMo/F2 have lower stacking than the CoMo/M1 and CoMo/M2 catalysts, while CoMo/M2 shows a more uniform stacking.

3.5 Thermal programmed desorption of ammonia

The acidity analysis was performed using TPD of NH_3 adsorption because this molecule has higher basic strength than pyridine and an appropriate molecular size for diffusion inside of zeolite porous (Damjanović and Auroux 2009). The TPD experiment was carried out to determine the materials acidity in oxide state but without distinguishing between Brønsted or Lewis acid sites. The sulfided catalysts were not measured because it is well-known that sulfided Mo and W exhibit activity on hydrodenitrogenation, and for this reason, molecules such as NH_3 and Pyridine are not appropriate to differentiate between different catalytic sites.

The acidity analysis at Figure 7 showed that acid sites density behaved as follows: F2>M2>M1>F1. The values were in accordance with nominal values of Si/Al ratio in the present work (MFI= 15 and FAU=2.42) included in Table 3. It is worth to mention that M2 sample was a mix of two phases (MOR and MFI) as DRX results exhibited, where mordenite

structure crystallized with a Si/Al= 5 ratio. This mixture could decrease the Si/Al ratio in the sample, increasing the aluminum amount, that is probably why we observed higher acid sites density in this sample.

The acidity results of catalysts showed that weak acid sites predominated in all samples except the CoMo/M2 where the three type of acid sites, weak, medium and strong showed similar values.

The catalysts showed a very similar acid sites amount trend to displayed by supports materials. Almost all catalysts (with the CoMo/F2 exception) increased the acid sites amount suggesting that impregnated metals generated additional acid sites. On the other hand, the decrease of this feature displayed by CoMo/F2 shows that the acid sites developed by the metals addition were less than the coated acid sites by those. The above could be a consequence of low textural properties showed by the F2; it could be caused the impregnation of metals in the surface of support limiting the NH_3 molecule diffusion to a large quantity of bulk acid sites.

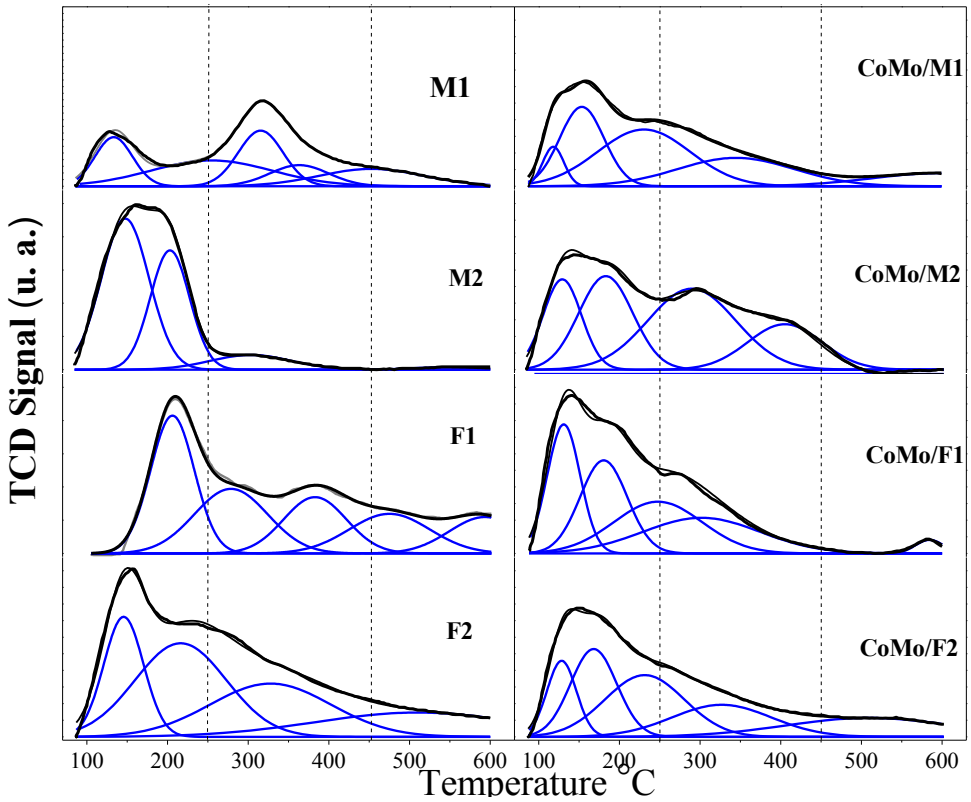

Fig. 7. TPD-NH_3 analysis for supports and catalysts precursors.

Table 3. The acidity of supports and oxide catalysts.

Sample	Acid centers (mmol NH_3 $gcat^{-1}$)			Total acid centers (mmol NH_3 $gcat^{-1}$)	Nominal Si/Al ratio
	Weak 100-250 °C	Medium 250-450 °C	Strong 450-600 °C		
M1	0.04	0.16	0.04	0.25	15
M2	0.28	0.03	0	0.31	15
F1	0.1	0.14	0.1	0.34	2.4
F2	0.32	0.15	0.12	0.59	2.4
CoMo/M1	0.23	0.08	0.04	0.35	15
CoMo/M2	0.22	0.23	0.02	0.47	15
CoMo/F1	0.24	0.17	0.01	0.42	2.4
CoMo/F2	0.27	0.08	0.07	0.41	2.4

3.6 DRIFT spectra of adsorbed NO

The NO molecule is the most frequently used adsorbate for characterization of hydrotreating catalysts. It is widely accepted that it can be used as a probe of anion vacancies (coordinatively unsaturated sites) on sulfide phases of unpromoted Mo, W based catalysts as well as those promoted with Co and Ni (Topsoe and Topsoe 1983). The NO molecules adsorbed as dinitrosyl species shows vibrational modes at 1800-1815 and 1700-1715 cm^{-1}. The first range is for symmetric stretching vibration mode and the second one corresponds to asymmetrical stretching vibration mode (Portela *et al.*, 1995). The NO molecule adsorbed on Co^{2+} ions shows a band at 1800-1880 and 1750-1800 cm-1 corresponding to symmetric and asymmetric stretching vibrations, respectively (Topsoe and Topsoe 1982). From this, we can notice that NO asymmetric and symmetric vibration modes on Co^{2+} and $Mo^{\delta+}$ respectively overlap each other. The sulfided samples show a shift toward lower wavenumbers; the difference in shift amplitude can be a consequence of the electronegativity difference between oxygen and sulfur (Zepeda, 2008).

In Figure 8 are shown the DRIFT signals of NO adsorbed on sulfided catalysts. All spectra were divided into two zones; zone I correspond to the 1600-1750 cm^{-1} range and zone II to the 1750-1950 cm^{-1}. The peaks observed at 1647-1670 cm^{-1} in the zone I are produced by the asymmetric stretching vibrations of reduced $Mo^{\delta+}$ species while peaks in zone II are produced by NO adsorbed on Co^{2+} sulfided or not. Thus, 1816 cm^{-1} signal was produced by NO molecule on Co^{2+} while signals at 1864 and 1900 cm^{-1} were produced by Co^{2+} symmetric stretching vibration modes for sulfided and some oxide species respectively, suggesting that an incomplete sulfidation of cobalt occurred.

According to the relative intensity of NO adsorbed signals, the CoMo/M1 sample showed the highest amount of NO adsorbed on the sulfide Co species in comparison with the other samples. The following order was observed: CoMo/M1 > CoMo/M2 > CoMo/F1 > CoMo/F2. The relative intensity of NO adsorbed on Co was higher than on Mo, however as the Mo concentration was higher than Co we can conclude that Co had a strong interaction with the MoS_2 phase (promotion effect). In this sense, we can expect a better promotion of MoS_2 by Co for the CoMo/M1 and CoMo/M2 catalysts, especially the CoMo/M1 catalyst which presented the highest HDS activity.

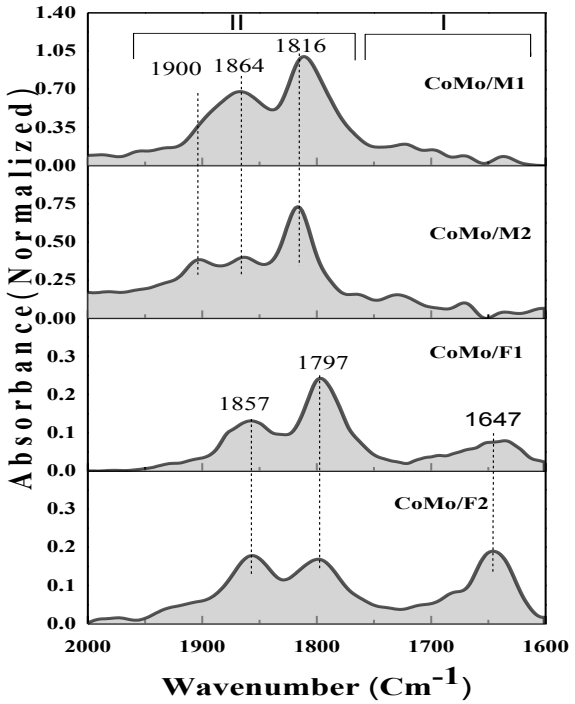

Fig. 8. DRIFT spectra for NO adsorption on sulfided catalysts.

In the same way, the non-appearance or low signal of NO adsorbed on Mo on these CoMo/M1 and CoMo/M2 catalysts reinforces the idea that Co promoted to the MoS_2 phase. Finally, the appearance of NO adsorbed on cobalt oxide species indicated that some fractions of Co ions are not completely sulfided under conditions used in this work.

4 Discussion

4.1 Supports

Hierarchical supports based on zeolites MFI, mordenite, and faujasite, were obtained by modification of the zeolite synthesis method using the addition of DM0TOPC and CTAB-PEG which allowed to create mesoporosity. The use of DMOTPAC brought to clear mesoporosity creation in M1 and F1 materials; while CTAB-PEG system resulted in a low mesoporous material (F2) and an interesting mesoporous material (M2) which grew up as bonded nanorods, presenting mesoporosity derived of inter-nanorod spaces. This result is similar to that reported by Shetti *et al.*, (2008) for ZSM 5. They showed that use of mesopore creating agent was appropriate to create additional porosity. Also,

Ismagilov *et al.*, (2009) showed that textural properties were improved considerably for these types of zeolite structures, ZSM 5 and Faujasite.

The XRD diffraction patterns of M1 and F1 materials showed highly crystalline mesoporous MFI and Faujasite, respectively; while F2 sample showed high crystallinity Faujasite but low mesoporosity. This indicates that DMOTPAC and CTAB-PEG induced different morphologies probably due to the formation of micellar and lamellar precursors, respectively (Shetti *et al.*, 2008; Christiansen *et al.*, 2001; Wang & Exarhos 2003) which differently grew. Otherwise, the M2 diffraction pattern indicating intergrowth MOR/MFI that can be a consequence of the alkalinity strength. Due to NaOH used for the synthesis as has been reported by Shiralkar & Clearfield (1989) the coexistence mordenite, ZSM-5 and α-quartz in the same material was revealed. The relative amount of each phase depends on the Si/Al ratio, concentrations of salts and basicity of the solution. In this sense, it has been suggested that the mechanisms governing the kinetics processes of zeolite formation are related to the competition of species in the synthesis medium (Espejel-Ayala *et al.*, 2014). We suggest that this phenomenon happens in the presence of basic building units 5-1 of Mor since they appeared on both structures (Mordenite and ZSM-5) facilitating the MOR/MFI intergrowth (Baerlocher & McCusker 1996).

The textural properties disclosed that the total pore volume (Vp) in M1, M2, and F1 had a significant contribution of the mesostructure while in F2 showed less contribution. Probably for F2 the mesopore agent was not appropriate. In this sense Choi *et al.*, propose that crystalline zeolites containing both micro and mesoporous structure are difficult to obtain using conventional organic surfactants and molecular templates because phases separation phenomenon could happen. In such case, the surfactants are expelled from the aluminosilicate domain during the zeolite crystallization process, making it difficult to obtain mesostructured zeolites (Choi *et al.*, 2006).

4.2 Catalysts

The catalysts XRD analysis did not show diffraction signals of impregnated Co or Mo oxide phases indicating that particles had a good dispersion and a small crystal size that was below the limits of this technique.

The catalytic activity of catalysts in hydrodesulfurization of dibenzothiophene presented the trend: CoMo/M1> CoMo/M2> CoMo/F2> CoMo/F1. The catalysts showed a clear preference to direct desulfurization pathway (Figure 9A). The DDS selectivity can be related to Brønsted sites of the support and MoS_2 edge active sites. Brønsted sites act as proton donors to sulfided particles, and it could lead to C-S bond breaking (Mohanty *et al.*, 2012) while edge MoS_2 active sites are promoted by small slabs length and high slab stacking. When the edge MoS_2 sites interact with reactants using perpendicular adsorption of sulfur atoms, then direct desulfurization occurs (A. Duan *et al.*, 2015).

TEM analysis data provided the $\overline{L}$ and $\overline{N}$ values (Figure 6). The calculated parameters followed the next trend: CoMo/M2> CoMo/M1> CoMo/F1> CoMo/F2, while DDS activity behaved as follow: CoMo/M1> CoMo/M2> CoMo/F1> CoMo/F2. In general, we observed that materials showing higher values, displayed higher HDS activity as showed in Figure 9. These trends show that catalysts showing a larger stacking had higher amount of edge sites which resulted in a higher amount of sites responsible for direct desulfurization as Daage & Chianelli (1994) proposed in their rim-edge model.

The statistics of MoS_2 slab length and stacking in CoMo/M2 were related with the interparticle mesoporosity between the arrays of nanorods instead of the intraparticle mesoporosity generated by the DMTOPAC and CTAB-PEG mesoporogens causing that MoS_2 nanoparticles rise larger on M2 than in other supports. So a linear correlation can be proposed between the lengths and stacking of slabs with the HDS activity (Figure 10)

The total amount of acid sites showed the trend F2>F1>M2>M1 which was inverse to the HDS activity M1>M2>F2>F1(Figure 9B), the average slab length and the stacking number M1>M2>F1>F2 (Figure 10). Thus, the highest the acid sites amount the lower the slab length. The stacking degree also seemed to be correlated with the acid strength of supports which is mainly controlled by the crystal type as MOR>MFI>FAU (Miyamoto *et al.*, 1998; Niwa *et al.*, 1992), in particular by the micropore size restrictions. In this sense, we can see that higher acid strength produced more stacking of the active phases such as been proposed with nanobeta zeolite (Yao *et al.*, 2012). Otherwise, it can be seen that a higher acid sites density resulted in shorter slabs and lower stacking of active phases; this was due to a larger acid sites availability which can form bonds with active phase promoting a better dispersion.

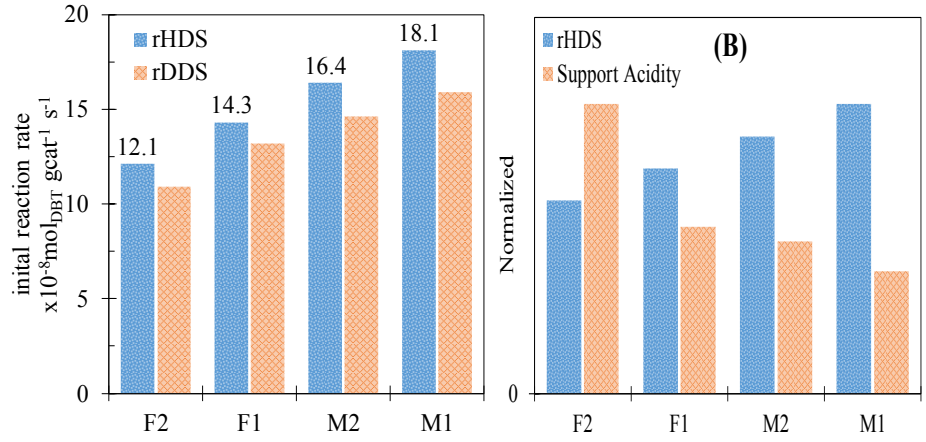

Fig. 9. (A). Correlation of reaction rates in HDS and the DDS pathway (rDDS is specific reaction rate in DDS pathway) presented by catalysts. (B) Correlation of normalized supports acidity and HDS reaction rates.

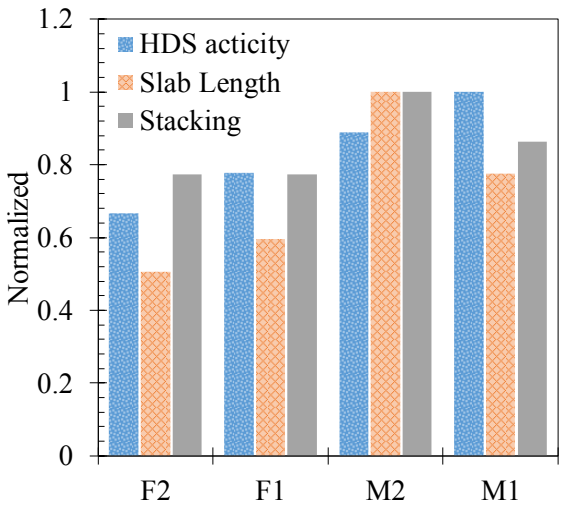

Fig. 10. Correlation between the normalized slab length, stacking and the catalytic activity.

From the relative intensities NO adsorbed measured by DRIFT on the catalysts the following order was observed: CoMo/M1 > CoMo/M2 > CoMo/F1 > CoMo/F2. This order indicated the importance of the promoter effect of Co on MoS_2 and it was in good agreement with the relative trend of catalytic activity for HDS. As a consequence of a better promotion of the MoS_2 phase an increase in the DDS pathway the catalytic activity directly is expected such as has been proposed by Diaz de Leon *et al.*, (2012). Therefore, a good correlation was established between the promoter effect of Co measured by NO adsorption, the DDS selectivity, and the HDS activity.

Conclusions

The supports showed suitable textural properties to disperse CoMoS sites on their surface. The use of mesoporogens DMOTPAC and CTAB-PEG allowed the appearance of mesopores in the 3.8 to 4.0 nm range which was favorable for HDS of DBT. The M1 and F1 support materials presented a very uniform mesoporous size system due to DMOTPAC usage. On the other hand, F2 showed low mesoporosity creation due to CTAB-PEG system. However, M2 sample displayed better textural properties due to nanorod interparticle mesopores.

There was evidence that the total acidity of supports impacted over the length and stacking of catalyst active phase; in this sense, we observed that the highest the acid sites amount, the lowest the slab length; conversely, the higher the acid strength, the higher the MoS_2 stacking. The increased stacking led to an increase of the DDS selectivity, according to proposed models (Daage & Chianelli 1994) indicating that direct desulfurization sites were located on the border of MoS_2 crystallites. Also, a good correlation was established between the intensity of NO adsorbed on Co by DRIFT, the HDS activity, and the DDS selectivity, confirming the importance of the CoMoS sites.

Acknowledgements

The authors are grateful to SENER-CONACyT for financial support through Project 117373, and wish to thank E. Aparicio, I. Gradilla, E. Flores, P. Casillas

and F. Ruiz for valuable technical assistance. R.I.Y acknowledges CONACyT for Ph.D. fellowship grant.

References

Alonso-Nunez, G., Bocarando, J., Huirache-Acuna, R., Alvarez-Contreras, L., Huang, Z. D., & Bensch, W. (2012). Influence of the activation atmosphere on the hydrodesulfurization of Co-Mo/SBA-15 catalysts prepared from sulfur-containing precursors. *Applied Catalysis a-General 419*, 95-101.

Baerlocher, C., & McCusker, L. B. (1996). Database of zeolites structures. Available in: http://www.iza-structure.org/databases/.

Breysse, M., Afanasiev, P., Geantet, C., & Vrinat, M. (2003). Overview of support effects in hydrotreating catalysts. *Catalysis Today 86*, 5-16.

Cervantes-Gaxiola, M. E., Arroyo-Albiter, M., Pérez-Larios, A., Balbuena, P. B., & Espino-Valencia, J. (2013). Experimental and theoretical study of NiMoW, NiMo, and NiW sulfide catalysts supported on an AlTiMg mixed oxide during the hydrodesulfurization of dibenzothiophene. *Fuel 113*, 733-743.

Corma, A., Martínez-Soria, V., & Schnoeveld, E. (2000). Alkylation of benzene with short-chain olefins over MCM-22 zeolite: Catalytic behaviour and kinetic mechanism. *Journal of Catalysis 192*, 163-173.

Cruz Pérez, A. E., Torrez Jiménez, Y., Velasco Alejo, J. J., Zepeda, T. A., Frías Márquez, D. M., & Rivera Ruedas, M. G. (2016). NiW/MgO-TiO_2 catalysts for dibenzothiophene hydrodesulfurization: Effect of preparation method. *Catalysis Today 271*, 28-34.

Chica, A., Diaz, U., Fornes, V., & Corma, A. (2009). Changing the hydroisomerization to hydrocracking ratio of long chain alkanes by varying the level of delamination in zeolitic (ITQ-6) materials. *Catalysis Today 147*, 179-185.

Choi, K.-H., Korai, Y., & Mochida, I. (2004). Preparation and characterization of nano-sized CoMo/Al_2O_3 catalyst for hydrodesulfurization. *Applied Catalysis A: General 260*, 229-236.

Choi, M., Cho, H. S., Srivastava, R., Venkatesan, C., Choi, D. H., & Ryoo, R. (2006). Amphiphilic organosilane-directed synthesis of crystalline zeolite with tunable mesoporosity. *Nature Materials 5*, 718-723.

Choi, M., Na, K., & Ryoo, R. (2009). The synthesis of a hierarchically porous BEA zeolite via pseudomorphic crystallization. *Chemical Communications*, 2845-2847.

Christensen, C. H., Johannsen, K., Schmidt, I., & Christensen, C. H. (2003). Catalytic benzene alkylation over mesoporous zeolite single crystals: Improving activity and selectivity with a new family of porous materials. *Journal of the American Chemical Society 125*, 13370-13371.

Christiansen, S. C., Zhao, D. Y., Janicke, M. T., Landry, C. C., Stucky, G. D., & Chmelka, B. F. (2001). Molecularly ordered inorganic frameworks in layered silicate surfactant mesophases. *Journal of the American Chemical Society 123*, 4519-4529.

Ginter, D. M., Bell, A. T., & Radke, C. J. (1992). *Synthesis of Microporous Materials*, New York: Van Nostrand Reinhold.

Daage, M., & Chianelli, R. R. (1994). Structure-function relations in molybdenum sulfide catalysts - the rim-edge model. *Journal of Catalysis 149*, 414-427.

Damjanović, L., & Auroux, A. (2009). Determination of acid/base properties by temperature programmed desorption (TPD) and adsorption calorimetry. In: *Zeolite Characterization and Catalysis: A Tutorial* (A. W. Chester, & E. G. Derouane, Eds.), Pp. 107-167. Dordrecht: Springer Netherlands.

De Leon, J. N. D., Petranovskii, V., de los Reyes, J. A., Alonso-Nunez, G., Zepeda, T. A., & Fuentes, S. (2014). One dimensional (1D) gamma-alumina nanorod linked networks: Synthesis, characterization and application. *Applied Catalysis a-General 472*, 1-10.

Díaz de León, J. N. (2016). Binary γ-Al_2O_3-α-Ga_2O_3 as supports of NiW catalysts for hydrocarbon sulfur removal. *Applied Catalysis B: Environmental 181*, 524-533.

Díaz de León, J. N., Picquart, M., Villarroel, M., Vrinat, M., Gil Llambias, F. J., & Murrieta, F. (2010). Effect of gallium as an additive in hydrodesulfurization WS_2/γ-Al_2O_3 catalysts. *Journal of Molecular Catalysis A: Chemical 323*, 1-6.

Díaz de León, J. N., Picquart, N., Massin, L., Vrinat, M., & de los Reyes, J. A. (2012). Hydrodesulfurization of sulfur refractory compounds: Effect of dallium as an additive in NiWS/γ-Al_2O_3 catalysts. *Journal of Molecular Catalysis A: Chemical 363*, 311-321.

Duan, A., Li, T., Zhao, Z., Liu, B., Zhou, X., & Jiang, G.(2015). Synthesis of hierarchically porous L-KIT-6 silica-alumina material and the super catalytic performances for hydrodesulfurization of benzothiophene. *Applied Catalysis B-Environmental 165*, 763-773.

Duan, A. J., Gao, Z. Y., Huo, Q., Wang, C. Y., Zhang, D. Q., & Jin, M. C.(2010). Preparation and evaluation of the composite containing USL zeolite-supported NiW catalysts for hydrotreating of FCC diesel. *Energy & Fuels 24*, 796-803.

Dugulan, A. I., van Veen, J. A. R., & Hensen, E. J. M. (2013). On the structure and hydrotreating performance of carbon-supported CoMo- and NiMo-sulfides. *Applied Catalysis B-Environmental 142*, 178-186.

Egeblad, K., Christensen, C. H., Kustova, M., & Christensen, C. H. (2008). Templating mesoporous zeolites. *Chemistry of Materials 20*, 946-960.

Espejel-Ayala, F., Solís-López, M., Schouwenaars, R., & Ramírez-Zamora, R. M. (2015). Synthesis of zeolite P using copper mining tailings. *Revista Mexicana de Ingeniería Quimica 14*, 205-212.

Diario Oficial de la Federación (2016). Available in: http://www.dof.gob.mx/nota_detalle.php?codigo=5450011&fecha=29/08/2016.

Feng, X., & Keith Hall, W. (1997). FeZSM-5: A durable SCR catalyst for NOx removal from combustion streams. *Journal of Catalysis 166*, 368-376.

Fujikawa, T., Chiyoda, O., Tsukagoshi, M., Idei, K., Takehara, S. (1998). Development of a high activity HDS catalyst for diesel fuel: from basic research to commercial experience. *Catalysis Today 45*, 307-312.

Gates, B. C., Katzer, J. R., & Schuit, G. C. A. (1979). *Chemistry of Catalytic Processes*: McGraw-Hill, New York.

Groen, J. C., Zhu, W. D., Brouwer, S., Huynink, S. J., Kapteijn, F., & Moulijn, J. A. (2007). Direct demonstration of enhanced diffusion in mesoporous ZSM-5 zeolite obtained via controlled desilication. *Journal of the American Chemical Society 129*, 355-360.

H. Topsøe, B.S. Clausen, & Massoth, F. E. (1996). *Hydrotreating Catalysis-Catalysis, Science and Technology*. Springer-Verlag, Berlin.

Huirache-Acuna, R., Rivera-Munoz, E. M., Pawelec, B., Ostrooumov, M., Maya-Yescas, R., & Rico, J. L. (2014). The use of a natural Mexican zeolite as support of NiMoW sulphide hydrotreating catalysts. *Catalysis Today 220*, 301-309.

Ishida, H. (1997). Liquid-phase hydration process of cyclohexene with zeolites. *Catalysis Surveys from Asia 1*, 241-246.

Ismagilov, Z. R., Yashnik, S. A., Startsev, A. N., Boronin, A. I., Stadnichenko, A. I., & Kriventsov, V. V. (2009). Deep desulphurization of diesel fuels on bifunctional monolithic nanostructured Pt-zeolite catalysts. *Catalysis Today 144*, 235-250.

Iwamoto, M., Yahiro, H., Tanda, K., Mizuno, N., Mine, Y., & Kagawa, S. (1991). Removal of nitrogen monoxide through a novel catalytic process. 1. Decomposition on excessively copper-ion-exchanged ZSM-5 zeolites. *The Journal of Physical Chemistry 95*, 3727-3730.

Jentoft, R. E., Tsapatsis, M., Davis, M. E., & Gates, B. C. (1998). Platinum clusters supported in zeolite LTL: Influence of catalyst morphology on performance inn-hexane reforming. *Journal of Catalysis 179*, 565-580.

Knudsen, K. G., Cooper, B. H., & Topsøe, H. (1999). Catalyst and process technologies for ultra low sulfur diesel. *Applied Catalysis A: General 189*, 205-215.

Lei, Q., Zhao, T. B., Li, F. Y., Zhang, L. L., & Wang, Y. (2006). Catalytic cracking of large molecules over hierarchical zeolites. *Chemical Communications*, 1769-1771.

Mei, C. S., Wen, P. Y., Liu, Z. C., Liu, H. X., Wang, Y. D., & Yang, W. M. (2008). Selective production of propylene from methanol: Mesoporosity development in high silica HZSM-5. *Journal of Catalysis 258*, 243-249.

Miyamoto, T., Katada, N., Kim, J. H., & Niwa, M. (1998). Acidic property of MFI-type gallosilicate determined by temperature-programmed desorption of ammonia. *Journal of Physical Chemistry B 102*, 6738-6745.

Mohanty, S., Mouli, K. C., Soni, K., Adjaye, J., & Dalai, A. K. (2012). Catalytic hydrotreatment using NiMo/MAS catalysts synthesized from ZSM-5 nano-clusters. *Applied Catalysis a-General 419*, 1-12.

Moosavi, E. S., Dastgheib, S. A., & Karimzadeh, R. (2012). Adsorption of Thiophenic Compounds from Model Diesel Fuel Using Copper and Nickel Impregnated Activated Carbons. *Energies 5*, 4233-4250.

Morsli, A., Driole, M. F., Cacciaguerra, T., Arletti, R., Chiche, B., & Hamidi, F. (2007). Microporosity of the amorphous aluminosilicate precursors of zeolites: The case of the gels of synthesis of mordenite. *Microporous and Mesoporous Materials 104*, 209-216.

Mungía-Guillén, J. L., Vernon-Carter, E. J., De los Reyes-Heredia, J. A., Viveros-García, T. (2016). Effect of surfactant in the synthesis of $CoMo/Al_2O_3$ catalysts obtained by reverse microemulsion for dibenzothiophene hydrodesulfurization. *Revista Mexicana de Ingeniería Química 15*, 893-902.

Niwa, M., Yamada, H., & Murakami, Y. (1992). Activity for the oxidation of methanol of a molybdena monolayer supported on Tin oxide. *Journal of Catalysis 134*, 331-339.

Pawelec, B., Halachev, T., Olivas, A., & Zepeda, T. A. (2008). Impact of preparation method and support modification on the activity of mesoporous hydrotreating CoMo catalysts. *Applied Catalysis a-General 348*, 30-41.

Perez-Ramirez, J., Christensen, C. H., Egeblad, K., Christensen, C. H., & Groen, J. C. (2008). Hierarchical zeolites: enhanced utilisation of microporous crystals in catalysis by advances in materials design. *Chemical Society Reviews 37*, 2530-2542.

Portela, L., Grange, P., & Delmon, B. (1995). The adsorption of nitric-oxide on supported Co-Mo hydrodesulfurization catalysts - a review. *Catalysis Reviews-Science and Engineering 37*, 699-731.

Ramirez, J., Fuentes, S., Díaz, G., Vrinat, M., Breysse, M., & Lacroix, M. (1989). Hydrodesulphurization activity and characterization of sulphided molybdenum and cobalt-molybdenum catalysts: comparison of Alumina-, Silica-Alumina- and Titania-supported catalysts. *Applied Catalysis 52*, 211-224.

Scott, C. E., Perez-Zurita, M. J., Carbognani, L. A., Molero, H., Vitale, G., Guzman, H. J., & Pereira-Almao, P. (2015). Preparation of NiMoS nanoparticles for hydrotreating. *Catalysis Today 250*, 21-27.

Serrano, D. P., Aguado, J., Escola, J. M., Rodriguez, J. M., & Peral, A. (2006). Hierarchical zeolites with enhanced textural and catalytic properties synthesized from organofunctionalized seeds. *Chemistry of Materials 18*, 2462-2464.

Shetti, V. N., Kim, J., Srivastava, R., Choi, M., & Ryoo, R. (2008). Assessment of the mesopore wall catalytic activities of MFI zeolite with mesoporous/microporous hierarchical structures. *Journal of Catalysis 254*, 296-303.

Shiralkar, V. P., & Clearfield, A. (1989). Synthesis of the molecular-sieve Zsm-5 without the aid of templates. *Zeolites 9*, 363-370.

Srivastava, R., Choi, M., & Ryoo, R. (2006). Mesoporous materials with zeolite framework: remarkable effect of the hierarchical structure for retardation of catalyst deactivation. *Chemical Communications*, 4489-4491.

Tang, T. D., Zhang, L., Fu, W. Q., Ma, Y. L., Xu, J., & Jiang, J.(2013). Design and synthesis of metal sulfide catalysts supported on zeolite nanofiber bundles with unprecedented hydrodesulfurization activities. *Journal of the American Chemical Society 135*, 11437-11440.

Tavizon-Pozos, J. A., Suarez-Toriello, V. A., de los Reyes, J. A., Guevara-Lara, A., Pawelec, B., & Fierro, J. L. G. (2016). Deep hydrodesulfurization of dibenzothiophenes over NiW sulfide catalysts supported on sol-gel titania-alumina. *Topics in Catalysis 59*, 241-251.

Topsoe, N. Y., & Topsoe, H. (1982). Adsorption studies on hydrodesulfurization catalysts. 1. Infrared and volumetric study of No adsorption on alumina-supported Co, Mo, and Co-Mo catalysts in their calcined state. *Journal of Catalysis 75*, 354-374.

Topsoe, N. Y., & Topsoe, H. (1983). Characterization of the structures and active-sites in sulfided Co-Mo/Al_2O_3 and Ni-Mo/Al_2O_3 catalysts by No chemisorption. *Journal of Catalysis 84*, 386-401.

Tosheva, L., & Valtchev, V. P. (2005). Nanozeolites: Synthesis, crystallization mechanism, and applications. *Chemistry of Material 17*, 2494-2513.

Trejo, F., Rana, M. S., Ancheyta, J., & Chavez, S. (2014). Influence of support and supported phases on catalytic functionalities of hydrotreating catalysts. *Fuel 138*, 104-110.

Wang, L. Q., & Exarhos, G. J. (2003). Study of local molecular ordering in layered surfactant-silicate mesophase composites. *Journal of Physical Chemistry B 107*, 443-450.

Yao, S. D., Zheng, Y., Ng, S. U., Ding, L. H., & Yang, H. (2012). The role of nanobeta zeolite in NiMo hydrotreating catalysts. *Applied Catalysis a-General 435*, 61-67.

Yoshinari, T., Usui, K., Yamamoto, Y., Ohi, M. Japan Patent 2 547 115, 1996, to Cosmo Oil Company and Petroleum Energy Center.

Zepeda, T. A. (2008). Comparison and performance of different sulphided Ti-loaded mesostructured silica-supported CoMo catalysts in deep HDS. *Applied Catalysis a-General 347*, 148-161.